Effects of a superconducting lead endcap on the magnetic field profile for the nEDM search

Aritra Biswas, with Filippone Group
Kellogg Radiation Laboratory, California Institute of Technology

Discovery of a non-zero electric dipole moment in the neutron (nEDM) would indicate a CP violation, with implications for extending the Standard Model and confirming predictions about matter-antimatter asymmetry. Experiments using shifts in neutron precession frequency to measure the nEDM require a uniform magnetic field to prevent false signals. We investigate the effectiveness of a superconducting lead endcap in promoting field uniformity inside an open-ended cylindrical coil. Measured field maps in the superconducting state closely match simulations and indicate that the endcap causes field peaks to shift away from magnet center, decreasing field gradients in desired regions. Simulations also suggest that the endcap may prevent field effects caused by imperfections in the geometry of an axial lead shield that surrounds the coil.

I. MOTIVATION

CP violation plays a critical role in explaining matter-antimatter asymmetry in the universe and guiding theories beyond the Standard Model; as such, the search for instances of CP violation is ongoing.[1,2] A non-zero electric dipole moment (EDM) in the neutron would constitute such a violation and can be measured through the shift in Larmor precession frequency of neutrons in $\vec{E}$ and $\vec{B}$ fields.[3] An experimental limit of $|d_n| < 2.9 \times 10^{-26}\ e \cdot \text{cm}$ was established by ILL in 2006.[2]

Experiments using these methods are prone to a geometric phase (GP) effect, caused by gradients of the $\vec{B}$ field, that can lead to a false signal, i.e. the measurement of a non-zero EDM even if the real EDM is zero..[2,3] As part of an effort to improve the measured limit, we have construced a half-scale model of a neutron EDM (nEDM) measurement experiment, using new methods to minimize errors such as the GP effect. Preventing the GP requires precise engineering to create a space-uniform magnetic field. To accomplish this, we use a coil tuned to create an uniform magnetic field, surrounded by shielding made of ferromagnetic Metglas and superconducting lead.

Here, we introduce a new shielding component - a superconducting lead top endcap - into the half-scale model. We compare its effects on the magnetic field to simulations, predict its effect on field gradients in the volumes in which neutrons will travel in the full-scale nEDM experiment, and analyze the desirability of including a similar endcap in the full-scale experiment.

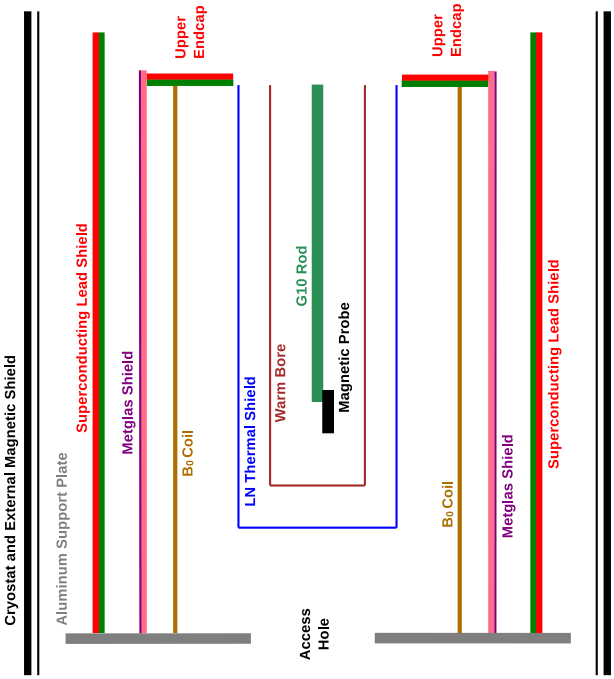

FIG. 1: Stylized diagram of the half-scale model, showing a vertical cross-section of the cylindrical apparatus. The vertically-oriented layers shown above - i.e. the cryostat shield, lead shield, Metglas shield, coil, thermal shield, and warm bore - are concentric cylinders nested inside one another. The G10 rod is shown along the z-axis: the common central axis of the cylinders. The endcap sits on top.

II. INTRODUCTION TO THE HALF-SCALE MODEL

At the center of the half-scale model (magnet center) are two fiducial 3.8 cm × 5 cm × 20 cm volumes. In the full-scale experiment, these volumes will be the measurement cells in which precession measurements of trapped ultra-cold neutrons (UCN) will take place, so the goal is to achieve field uniformity within.

The magnetic field is generated by the B_0 coil, a cylindrical structure with wires along its surface in a $\cos\theta$ coil geometry that creates a magnetic field orthogonal to the cylinder's central axis.[6] Concentric cylindrical shielding structures (shown in Figure 1) surround the B_0 coil; cylinders are nested one inside the other in a structure resembling "Russian dolls."

We define the z-axis as the common central axis of these cylinders, and the x-axis as the primary direction

of the magnetic field.

The B_0 coil, of course, cannot create a sufficiently uniform field without the surrounding shielding. The ferromagnetic Metglas shield redirects the field and promotes uniformity near magnet center. The cylindrical superconducting lead shield (axial shield) protects the field from environmental gradients and fluctuations.

The lead endcap (the focus of this study) has an annular cross-section and lays on top of the cylindrical shields. We include it in an attempt to mitigate edge effects of the magnetic field; expectations of the endcap's behavior are discussed further in the next section.

The whole apparatus is placed inside a cryostat capable of bringing the lead components (the axial shield and the endcap) to 4 K. A thermal shield and warm bore are placed in the center: the warm bore is kept at room temperature and contains the magnetic probe.

III. EXPECTATIONS OF ENDCAP BEHAVIOR

Without the endcap, we expect the field near the open ends of the B_0 coil to exhibit edge effects similar to those shown in Figure 2a. The obvious correction is a circular endcap covering the open area, but since the center must be left open for access by the magnetic probe, we used an annular design. Figure 2b shows the expected influence on the field's edge effects.

Simulations of the half-scale model with `RotationShield`, a matrix solver developed previously in the group,[7] offer more precise predictions. Since the desired field points in the x direction and edge effects push the field in the z direction, examining B_x and B_z as a function of z near the height of the endcap ($z = 1.128$ m) offers insight into the endcap's effects. It is important to note that this curve is interesting only away from the central axis, since $B_z = 0$ everywhere along the central axis; this is apparent in the sketches (Figure 2) and corroborated by simulations. Figure 3 compares simulated field maps without and with an endcap along the off-axis line $x = 0.1$ m, $y = 0$, showing the expectation that the endcap will shift the peak in B_z to higher z (away from magnet center as desired).

IV. MEASUREMENT METHODS AND CORRECTIONS

Field maps can be collected by moving the magnetic probe around the warm bore with a 3-axis stepper motor. We focus on three configurations: (A) axial shield and endcap in non-superconducting states; (B) axial shield in a superconducting state, endcap in a normal state; and (C) axial shield and endcap in superconducting states. With selective heating and cooling of components, we can bring the half-scale model to each of these three configurations.

The resulting field maps, if directly compared to simulations, reveal many discrepancies that result from measurement errors. Each of these errors, and relevant corrections, are addressed below.

A. Background subtraction

For each map, we must measure the background magnetic field (i.e. when the B_0 coil is turned off) and subtract this field from the foreground (B_0 on). This step allows us to isolate the effects of our changes in shielding geometry.

B. Probe centering

We have found that the field profile is highly sensitive to x position. For example, along the cylinder's central axis ($x = 0, y = 0$), simulations predict that B_z should be 0; however, when $x \neq 0$, the B_z vs. z curve exhibits a peak near $z = 1.073$ m, the end of the B_0 coil. The height of this peak is directly correlated with the x position. Early comparisons showed a B_z vs. z peak even along $x = 0, y = 0$, and measurements confirmed that the probe setup is not correctly centered along the x axis. Since such centering is difficult, we measure the offset and correct for it during data analysis. For example, consider a mapping where the probe is offset by 4 mm along the positive x direction. Data taken along $x = 0.1$ m, after correction, is recognized as data taken along $x = 0.104$ m, so we can compare the curve to the appropriate simulated curve.

C. Probe offset

Our magnetic probe is composed of three separate one-axis probes which are separated along the z-axis. The probe's location corresponds to the location of the B_z probe: the B_x probe is 15 mm above this location, while the B_y probe is 15 mm below.. Thus when the probe location is read as $(0, 0, 0)$, the B_x probe, for example, is actually at $(0, 0, 0.015$ m$)$. The data that we collect cannot be expressed as a single vector map, then, since we are not guaranteed to have a vector (B_x, B_y, B_z) for every point (x, y, z). In the analysis programs, we implement spatial axes that are capable of storing an offset vector corresponding to the components of the field, such that the z axis can be offset depending on whether we are graphing B_x vs. z or B_z vs. z.

D. Probe tilt

The probe's rigid mount introduces another problem: the probe cannot be perfectly vertical. Since $B_x >> B_z$ at magnet center, even a very small angle can make the

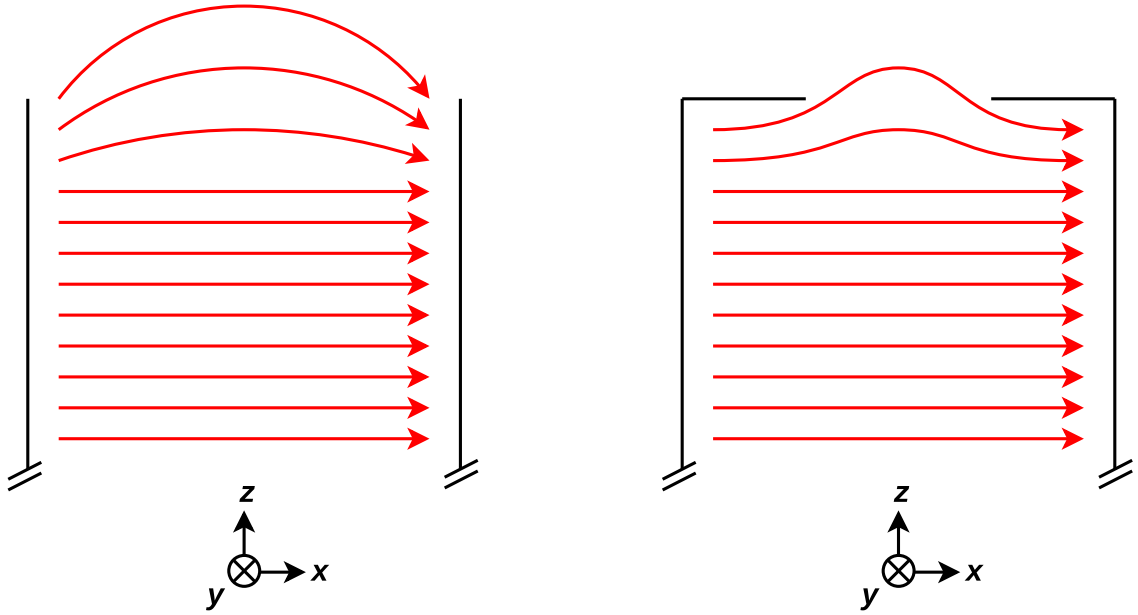

(a) (b)

FIG. 2: Sketches of the expected magnetic field without (2a) and with (2b) the endcap. The endcap is expected to mitigate the edge effects and point the field more uniformly along the x-axis.

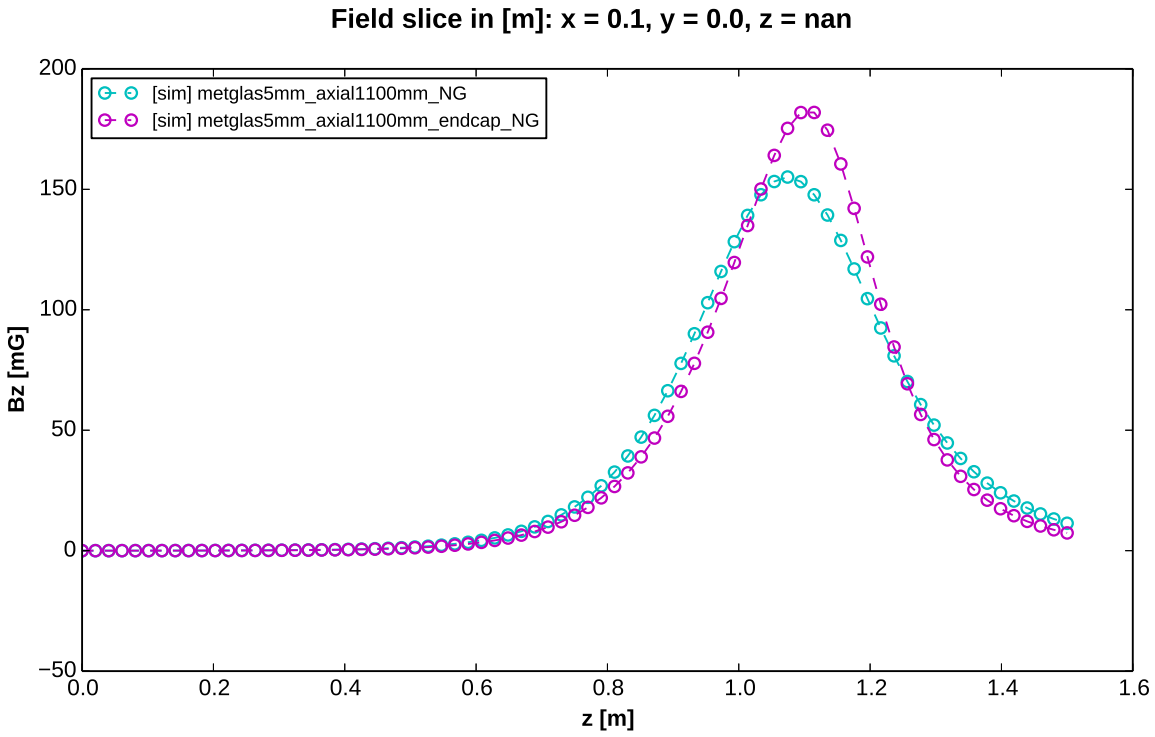

FIG. 3: B_z vs. z as predicted by simulations in two configurations: with the superconducting endcap (magenta curve) and without (cyan curve). The axial shield is present and superconducting in both curves.

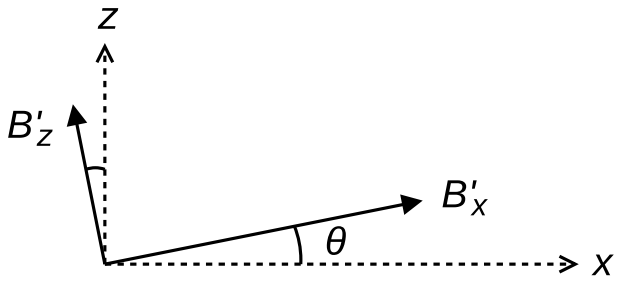

FIG. 4: A diagram of the probe tilt. The x and z axes are correct relative to the magnet. However, because the probe is tilted at some angle θ, the given B'_x and B'_z are misaligned.

B_z probe pick up part of the B_x signal; this effect is illustrated in Figure 4. The probe, tilted at some angle θ, gives skewed readings B'_x and B'_z. The true readings B_x and B_z can be obtained from the skewed readings B'_x and B'_z and the angle θ through simple trigonometry.

To determine θ, we observe that in simulations, $B_z = 0$ at magnet center, while measured field maps show a small nonzero B'_z at magnet center. Assuming that the main source of this error is the probe tilt, we can estimate the angle $\theta = -\frac{B'_z}{B'_x}$. We consider this a reasonable assumption since the difference $B'_z - B_z$ seems proportional to B_x; this coupling of the components suggests their values are skewed by the probe angle. Furthermore, we apply this correction last to ensure that probe tilt is the main remaining source of error.

E. Normalization

Simulation output from `RotationShield` gives the magnetic field in arbitrary units, so the expected magnetic field strength at any location is known only relative to another known location. To compare these simulations with our measured output, we draw a small cube around magnet centerin the measured map, calculate the average B_x inside, and normalize the simulated map such that B_x at its center matches the measured map. This adjustment allows fair comparison of absolute field strengths at any location.

F. Error bars

The magnetic probe provides error bars for each measurement point. All error bars in plotted curves were found to be below 0.2 mG, negligible in the following plots with ranges of 250 to 300 mG on the y-axis.

V. FIELD PROFILES

A. Axial shield normal, endcap normal

Before making predictions about the superconducting (SC) cases, comparing measurements with both lead components in a normal state to corresponding simulations offers insight into the discrepancies between the simulated and real systems. Initial versions of these comparisons reveal the need for the various aforementioned corrections.

Figure 5 shows simulated and measured B_z vs. z curves in the "normal, normal" case, demonstrating good agreement with simulations.

B. Axial shield superconducting, endcap normal

Upon activating the axial shield by bringing it to superconducting (SC) temperature, but leaving the endcap in a normal state, we expect minimal change in the field in the region that is being plotted for two reasons. First, the Metglas shield (whose main purpose is to enforce field uniformity) is already present, so the role of the axial shield is reduced. Second, by design, the axial lead shield has a greater effect on the field at magnet center. This study, however, focuses on the field near the top endcap, away from magnet center.

Figure 6 shows the simulated and measured curves for the "SC, normal" as well as the simulatede "normal, normal" curve from Figure 5. The simulated curves are almost indistinguishable, showing the expectation that the effect of the axial shield should be negligible. This expectation seems reasonable as the "SC, normal" measured curve shows minimal deviation from the simulations.

It is interesting to note that, according to simulations, this is not always the case. Figure 7 shows simulated curves for the "SC, normal" configuration with 5 mm variations in the height of the axial shield, along with a curve for the "normal, normal" configuration. When the axial shield's length is 1.100 m, the "SC, normal" curve seems indistinguishable from the "normal, normal" curve. A similar variation, where the axial shield height was held constant and the height of the Metglas shield was varied, yielded similar results. This suggests that the influence of the axial shield depends on the height difference between it and the Metglas shield - the further the axial shield extends above the Metglas, the more effectively it suppresses the B_z peak.

C. Axial shield superconducting, endcap superconducting

Figure 8 shows the same axial shield height variation as in Figure 7, but with the endcap included at a fixed height ($z = 1.128$ m) in each case, showing that the

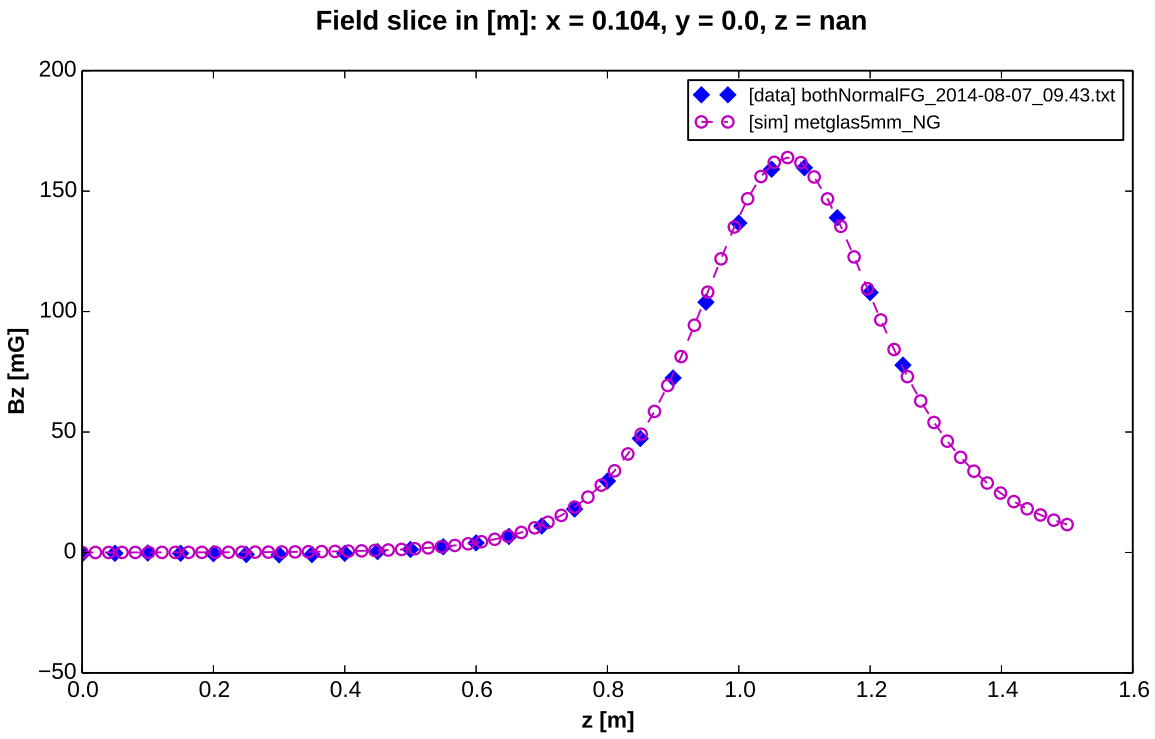

FIG. 5: Comparison of simulated and measured B_z vs. z curves with both the axial shield and the endcap in a normal state.

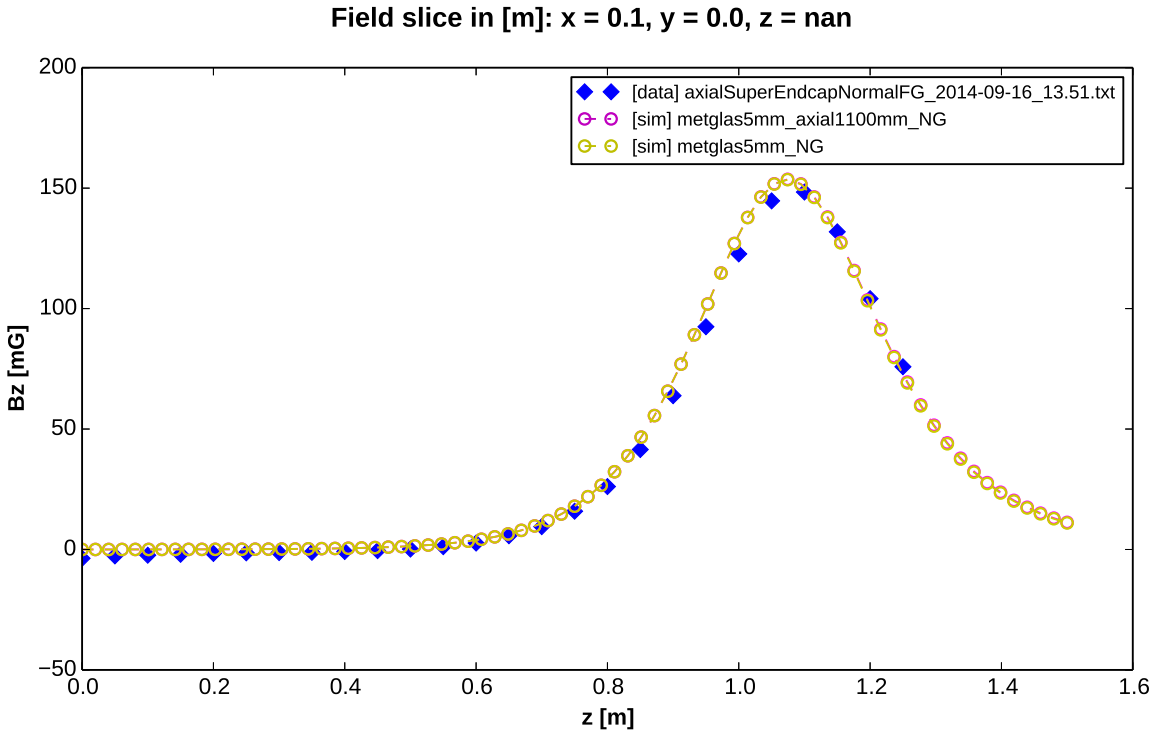

FIG. 6: Comparison of simulated and measured B_z vs. z curves with the axial shield superconducting, but the endcap in a normal state, overlaid with the simulated curve from Figure 5 to show agreement between the "normal, normal" and "SC, normal" cases.

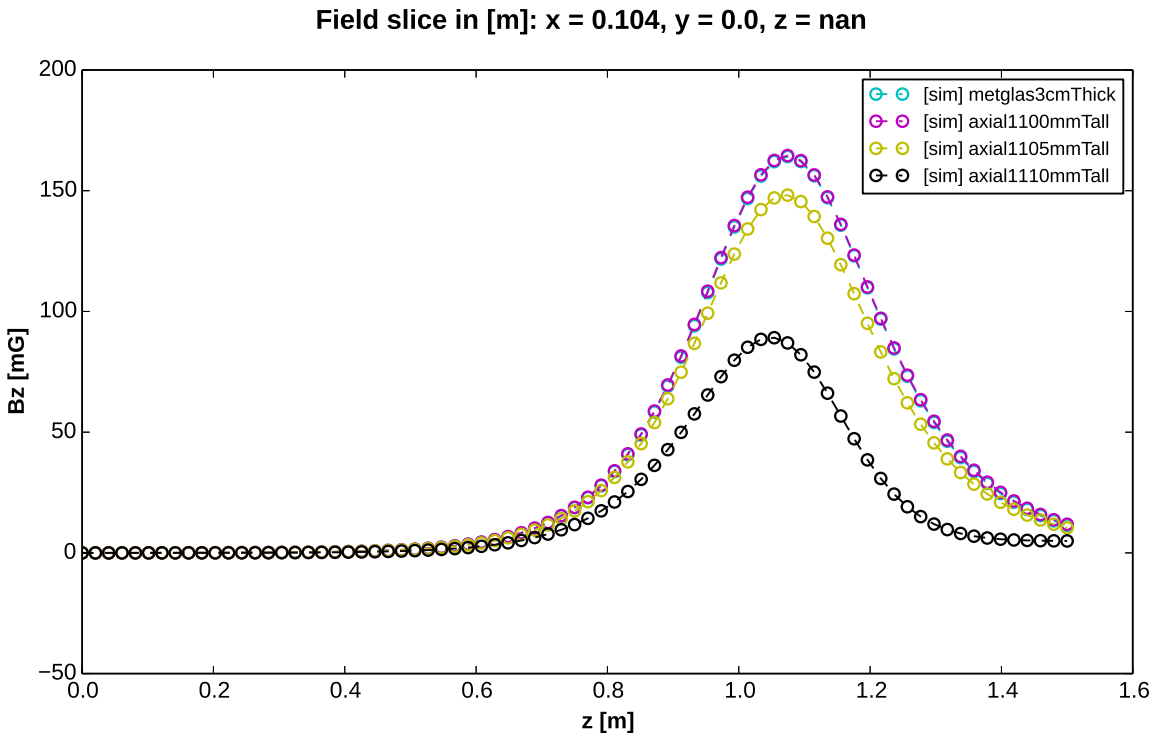

FIG. 7: B_z vs. z as predicted by simulations with variations in the height of the axial shield. The cyan curve (no axial shield) and the magenta curve (axial shield height at 1.100 m) are indistinguishable. Greater axial shield heights result in further suppression of the B_z peak.

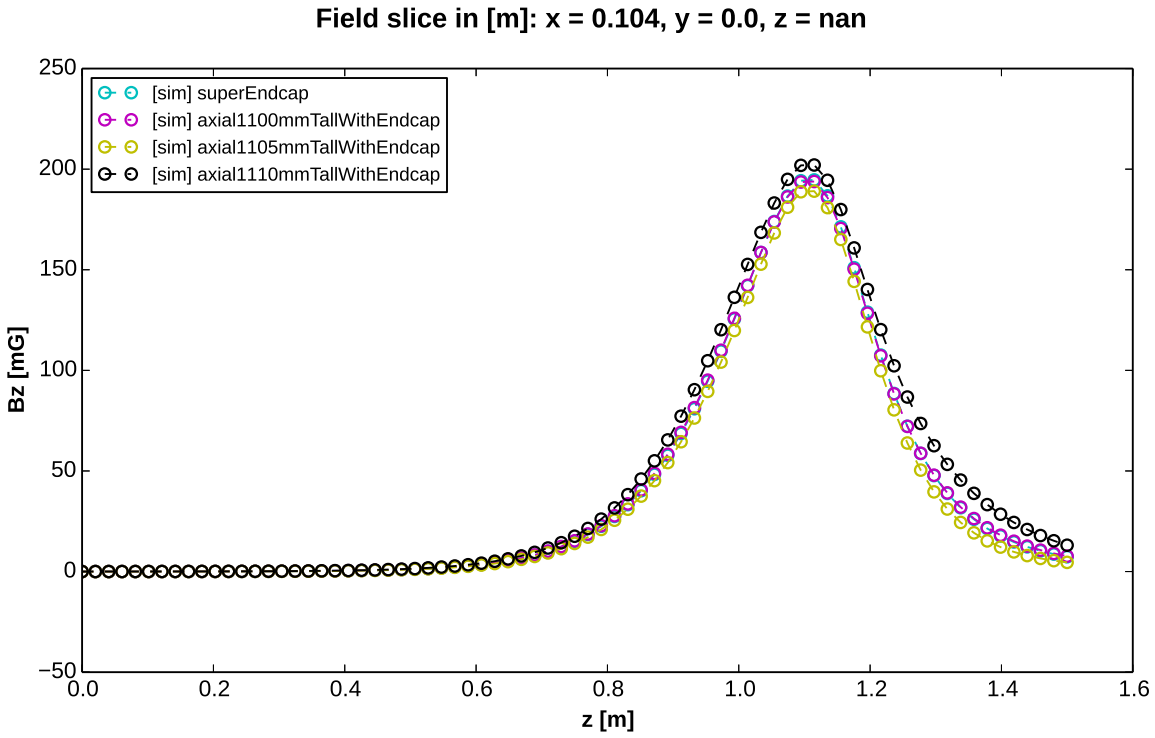

FIG. 8: B_z vs. z as predicted by simulations with the same variations in the height of the axial shield as in Figure 7, but with the superconducting endcap present. The suppression of the B_z peak is no longer visible.

curves that were clearly distinct without the endcap become harder to distinguish in the presence of the superconducting endcap.

In addition to the endcap's large-scale effects on field profiles, it is important to observe that its addition should not significantly alter field gradients in the measurement cell volumes. Table I shows volume-averaged components of the gradient of $\vec{B}$ in the measurement cell calculated from high-resolution simulations. These results suggest that we are justified in comparing field gradients with and without the endcap.

VI. ANALYSIS

Figures 5, 6, and 9 all show good agreement between measurement and simulation. As expected, the endcap shifts the B_z peak, a main source of non-uniformity, away from magnet center. Comparisons show that our simulations are effective at predicting the endcap behavior, motivating further simulated studies of different endcap geometries.

The study of simulations with varying axial shield heights (Figures 7 and 8) show that the expectation that the axial shield itself will not significantly alter the field only holds when the Metglas-axial shield height difference is small. That the axial shield exertts a stronger influence on the interior field when more of it is left "uncovered" by the Metglas shield is not surprising. However, Figure 8 clearly shows that the introduction of the superconducting endcap effectively hides the axial shield's direct influence on the field.

The tight agreement between the measured "normal, normal" and "SC, normal" cases seen in figure 6 indicates that, in our half-scale model, the Metglas-axial shield height difference is indeed sufficiently small. Introducing the endcap in these simulatiosn suggests that, even if our estimate of the Metglas-axial shield height difference is innacurate, the presence of the endcap could partially hide the effects of that error.

Furthermore, gradient changes expected due to the endcap (see I) are all well below 0.1 μG/cm, which suggests that good uniformity can be maintained with the endcap.

VII. ACKNOWLEDGMENTS

The author is grateful for support from the Arthur R. Adams SFP Fellowship.

[1] Cronin, J. "Nobel Lecture: CP Symmetry Violation The Search for Its Origin," Nobel Media AB (2013).

[2] Baker, C. A., D. D. Doyle, P. Geltenbort, K. Green, M. G. D. Van der Grinten, P. G. Harris, P. Iaydjiev et al. "Improved experimental limit on the electric dipole moment of the neutron." *Physical Review Letters* 97, no. 13 (2006): 131801.

[3] Pendlebury et. al. "Geometric-phase-induced false electric dipole moment signals for particles in traps." *Phys. Rev. A.* 70, 032102 (2004).

[4] "Search for the nEDM at Caltech." Kellogg Radiation Laboratory ⟨krl.caltech.edu⟩ (2014).

[5] Malkowski, S., R. Y. Adhikari, J. Boissevain, C. Daurer, B. W. Filippone, B. Hona, B. Plaster, D. Woods, and H. Yan. "Overlap Technique for End-Cap Seals on Cylindrical Magnetic Shields." *IEEE Transactions on Magnetics* 49, no. 1 (2013): 651-653.

[6] Perez Galvan, A., B. Plaster, J. Boissevain, R. Carr, B. W. Filippone, M. P. Mendenhall, R. Schmid, R. Alarcon, and S. Balascuta. "High uniformity magnetic coil for search of neutron electric dipole moment." *Nuclear Instruments and Methods in Physics Research Section A: Accelerators, Spectrometers, Detectors and Associated Equipment* 660, no. 1 (2011): 147-153.

[7] Mendenhall, M. P. `RotationShield` source. ⟨https://github.com/mpmendenhall/rotationshield⟩ (2014).

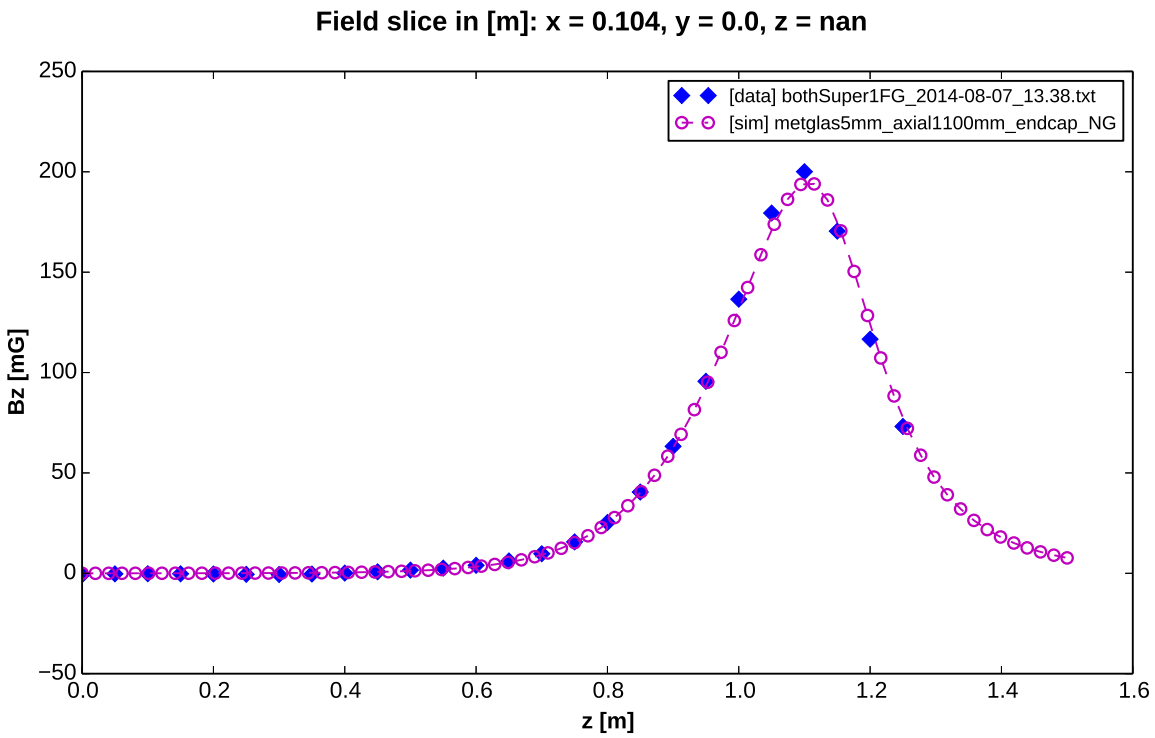

FIG. 9: Comparison of simulated and measured B_z vs. z curves with both the axial shield and the endcap in a superconducting state.

	"norm, norm"	**"SC, normal"**	**"SC, SC"**	**cap change**
$\partial B_x/\partial x$	-0.287690	-0.285294	-0.290683	0.005389
$\partial B_y/\partial x$	0.000005	-0.000020	-0.000115	0.000095
$\partial B_z/\partial x$	-0.000001	0.003045	0.030903	-0.027858
$\partial B_x/\partial y$	0.000001	0.000011	0.000009	0.000002
$\partial B_y/\partial y$	0.318764	0.317201	0.315975	0.001226
$\partial B_z/\partial y$	0.000001	0.000002	0.000001	0.000001
$\partial B_x/\partial z$	0.000000	-0.018646	-0.028932	0.010286
$\partial B_y/\partial z$	0.000001	-0.000002	-0.000021	0.000019
$\partial B_z/\partial z$	-0.039736	-0.041182	-0.037189	-0.003993

TABLE I: Simulated volume-averaged gradients in the measurement cell, in μG/cm, with a central field of 30 mG. "Cap change" is the change due to the endcap when the axial shield is already SC. Changes smaller than 0.1 μG/cm are negligible in measurement.